Title

Effects of leaf area index and density on ultrafine particle deposition onto forest canopies: A LES study

Authors

Lin, Xinlu
Chamecki, Marcelo
Katul, Gabriel
et al.

Publication Date

2018-09-01

DOI

10.1016/j.atmosenv.2018.06.048

Effects of Leaf Area Index and Density on Ultrafine Particle Deposition onto Forest Canopies: a LES Study

Xinlu Lin[a], Marcelo Chamecki[b,*], Gabriel Katul[c], Xiping Yu[a]

[a] *Department of Hydraulic Engineering, Tsinghua University, Beijing10084, China*
[b] *Department of Atmospheric and Oceanic Sciences, University of California, Los Angeles, Los Angeles, CA, USA*
[c] *Nicholas School of the Environment, Duke University, Durham, NC, USA*

Abstract

A framework to describe transport and deposition of ultrafine particles (UFP) within forests using large eddy simulation (LES) is presented. Comparison with measurements collected within and above a Scots pine stand in Southern Finland are used to explore the plausibility of the simulations. The numerical model is then employed to quantify the effects of canopy morphology (leaf area index and leaf area density), turbulence intensity, and particle size on the partitioning between upper canopy and subcanopy deposition and the overall deposition velocities. Results show a complex interplay between canopy morphology and turbulence, which is reflected on the particle flux profiles within the canopy. However, mean particle concentration profiles, total deposition, and deposition velocities at the canopy top are insensitive to the leaf area density profile but show dependence mostly on leaf area index, turbulence levels, and particle size. Finally, with the goal of understanding the sensitivity of the deposition velocity to all these parameters, an analytical model is developed that shows good agreement with LES results (within $\pm 20\%$) for all conditions simulated here.

Keywords: Large Eddy Simulation; LAD; LAI; Particle deposition; UFP

*Corresponding author
Email address: chamecki@ucla.edu (Marcelo Chamecki)

1. Introduction

Atmospheric concentrations of ultrafine particles (UFP, particles with diameter $d_p \leq 100\,\text{nm}$) have important effects on the climate system and air pollution. UFP are one of the main sources of cloud condensation nuclei in the atmosphere and are recognized to alter the reflectivity and life-time of clouds [1]. Inhalation of airborne UFP can contribute to adverse health effects both in the respiratory tract and extrapulmonary organs [28]. Understanding these effects requires information on all steps of UFP life-cycle in the atmosphere, including emission/formation, transformation, transport, and removal by wet and dry deposition [22]. Here, the focus is on UFP collection by vegetation given its significance in dry deposition [3].

Dry deposition of particles on vegetated surfaces depends primarily on particle size, turbulence above and within the vegetation layer, and the collection properties of the vegetation elements (such as leaves and branches) and soil surfaces [15]. For particles in the UFP range, for which gravitational settling and deposition by interception and impaction are negligible [32], the role of turbulent transport within the canopy layer and Brownian diffusion near the vegetation elements are the dominant processes. The development of measurement techniques and instrumentation that allow size-resolved eddy-covariance fluxes to be determined in field conditions has lead to progress in the understanding of dry deposition in forested environments [14, 15]. This knowledge is complemented by laboratory experiments investigating effects of leaf morphology and leaf area index (LAI) on particle removal [26, 19]. However, the interplay between vegetation structure and UFP removal continues to draw significant research attention [21, 20].

As an example, Vesala et al. [41] used eddy-covariance fluxes of particles (ranging in diameter between 3 nm and 500 nm) together with a model for the dependence of deposition velocity on particle size to evaluate the effect of forest thinning on deposition velocities. The authors found that a reduction in about 25% in total LAI (from LAI=8 to 6) resulted in a reduction of about 60% in the

deposition velocity when using the classical model by Slinn [39]. Katul et al. [20] used the same data set but a different modeling approach and arrived at a reduction of 25% for the deposition velocity, suggesting a direct proportionality between deposition velocity and LAI. Using branch-scale wind tunnel experiments for UFP, LAI was shown to be the key determinant of particle collection when compared to leaf area density shape [18] and that total particle collection scales with LAI. Studies of the effects of canopy architecture and turbulence levels on deposition of UFP are scarce and even the partitioning of deposition between the crown and the understory/ground remains a challenge [35]. Laboratory experiments with solid obstacles indicate that ground deposition can account for 20% to 60% of the total deposition [9]. This range is comparable with field experiments, which yield 10% to 35% [15]. However, Grönholm et al. [15] suggests that understory fraction decreases with increasing turbulence levels, while Donat and Ruck [9] observes the opposite.

A number of dry deposition models have been proposed and are currently in use for predicting UFP removal by vegetated surfaces [e.g. 39, 42, 33, 10]. Two reviews covering dry deposition onto vegetated canopies provide a summary of models and experiments reported over the past 30 years [32, 35]. Common in these reviews is the finding that even when size-resolved multilayered models of the canopy roughness sublayer are employed, significant deviations between modeled and measured deposition rates persist. A number of recent efforts have focused on development and use of multilayer size-resolved models that are not based on K-theory and are capable of representing the transport of UFP within different layers of the vegetation [17]. These models produce statistics in broad agreement with measurements, and suggest that both LAI and its vertical distribution (characterized by the leaf area density – LAD) are important in determining the deposition velocity above forests [20]. In addition, model calculations suggest that the partitioning between crown and understory/ground deposition is independent of the friction velocity, u_*[17]. Even though these models do not rely on K-theory, they also make a number of assumptions about turbulence and its interaction with the vegetation.

In the present work, large eddy simulation (LES) is used to explore the effects of particle size, turbulence intensity, and canopy architecture (represented by LAI and LAD) on the deposition of UFP to forests. In particular, the focus is on the partitioning between crown and understory/ground deposition and on the behavior of the deposition velocity as it varies with flow statistics. Simulations results are used as a guide in designing a reduced order analytical model that encapsules the key dependencies of the deposition velocity on particle size, canopy architecture and turbulence intensity. The LES approach is described in Section 2. Comparison with published field measurements and sensitivity simulations are presented in Section 3. The theoretical model is presented in Section 4, and conclusions are presented in Section 5.

2. Numerical Simulations

2.1. Flow through model canopy

The three-dimensional LES model employed in this study has been described in detail elsewhere [8, 29]. For brevity, only a few key features are highlighted here. The filtered momentum equation for neutral conditions is written as

$$\frac{\partial \tilde{\boldsymbol{u}}}{\partial t} + \tilde{\boldsymbol{u}} \cdot \nabla \tilde{\boldsymbol{u}} = -\frac{1}{\rho}\nabla \tilde{p} - \nabla \cdot \boldsymbol{\tau} + \boldsymbol{F}_d. \tag{1}$$

where $\tilde{\boldsymbol{u}}$ is the filtered velocity, $(1/\rho)\nabla\tilde{p}$ is the filtered pressure gradient force and $\boldsymbol{\tau}$ is the subgrid scale (SGS) momentum flux. A body force $\boldsymbol{F}_d$ is used to represent the additional drag forces imposed by the vegetation on the flow, as originally done by Shaw and Schumann [38] – see also discussion in Pan et al. [31]. It is assumed that pressure drag is dominant when compared to viscous drag and the force is modeled as

$$\boldsymbol{F}_d = -C_d(a\boldsymbol{P}) \cdot (|\tilde{\boldsymbol{u}}|\,\tilde{\boldsymbol{u}}) \tag{2}$$

where C_d is the drag coefficient (assumed to be constant), a is the overall leaf area density, and $\boldsymbol{P} = P_x \boldsymbol{e}_x\boldsymbol{e}_x + P_y\boldsymbol{e}_y\boldsymbol{e}_y + P_z\boldsymbol{e}_z\boldsymbol{e}_z$ is the projection coefficient tensor to project the leaf area density into streamwise (x), spanwise (y) and vertical (z) directions (here we use $C_d = 0.15$ and $P_x = P_y = P_z = 1/3$).

The momentum equations are solved in rotational form and discretized using a fully dealiased pseudo-spectral approach in the horizontal directions and a centered second-order finite-difference scheme in the vertical direction. The Lagrangian scale-dependent dynamic Smagorinsky SGS model [5] is employed to close the equations. A no-stress boundary condition is imposed at the top of the domain and a log-law wall model with imposed surface roughness is used to parameterize the bottom boundary condition at the soil surface. The flow is driven by a constant mean pressure gradient $dP/dx = u_s^2/L_z$, where u_s is a nominal velocity scale (that is close, but not identical, to the friction velocity) and L_z is the height of the domain. This model has been shown to produce first- second- and third-order flow statistics in agreement with measurements inside and above a cornfield [29] and an Amazon forest canopy [13].

2.2. Ultrafine particle transport and deposition

The simulation of ultrafine particle deposition onto canopy elements is undoubtedly complicated, and many simplifications are also required here for the problem to be tractable with existing information about canopy morphology and current computational resources. In fact, the problem is similar to that encountered for the flow field, for which the drag force resulting from interactions of the flow with individual leafs and branches cannot be explicitly represented in the simulation and a 'macroscopic' approach based on a body-force acting over an entire grid volume is necessary. In the same way, particle motion at the leaf scale cannot be represented explicitly in the model, and neither can the interaction of particles with the viscous boundary layer around individual plant elements. Thus, a macroscopic modeling approach must be sought.

In the approach developed here, UFP are assumed to be massless, in the sense that all effects associated with particle mass and inertia are neglected. In practice, this means that particles are transported by the turbulent wind field in the same way as a passive tracer (no gravitational settling and no inertial effects), and that the transport across laminar boundary layers around canopy elements and the ground is governed by Brownian motion (interception and

inertial impaction are negligible). These assumptions are well justified in the treatment of small particles in the UFP range [12, 32].

An Eulerian description that defines a particle concentration field as described in detail by Chamecki et al. [8] and Pan et al. [29] is used. In the present application, gravitational settling is not included in the model, and the particle concentration is advected only by the fluid velocity. The transport equation for particle concentration and deposition is written as

$$\frac{\partial \tilde{C}}{\partial t} + \nabla \cdot \left(\tilde{\boldsymbol{u}} \tilde{C} \right) = -\nabla \cdot \boldsymbol{\pi}^C - S_d, \tag{3}$$

where $\tilde{C}$ is the particle concentration, $\boldsymbol{\pi}^C$ is the SGS particle concentration flux, and S_d is the rate of particle deposition (or collection) onto canopy elements. The particle concentration field $\tilde{C}$ is assumed to be mono-dispersed, in the sense that all particles are assumed to have the same size in a given simulation. This assumption implies that $\tilde{C}$ can be defined either as number density (number of particles per unit volume) or as a mass density (total mass per unit volume), and it is important in designing a model for the particle deposition term. Because the present study focuses on UFP, canopy and ground deposition are controlled by Brownian diffusion across laminar boundary layers, requiring different parameterizations for S_d from those used by Chamecki et al. [8] and Pan et al. [29]. Following the general approach outlined by Friendlander [12], the canopy deposition S_d is modeled by

$$S_d = \alpha_g \tilde{C} \left(|\tilde{\boldsymbol{u}}| \, E_B \right). \tag{4}$$

Here, $\tilde{C}$ is the local instantaneous particle concentration and α_g is a geometric factor that includes the effects of leaf morphology and has units of inverse length (in all simulations presented here we use $\alpha_g = a/\pi$). This model is applicable to large Reynolds numbers in the range $10^2 < Re < 10^4$ (where $Re = |\tilde{u}| \, d_l/\nu$ is the Reynolds number of the flow around vegetation elements with characteristic dimension d_l). The collection efficiency for Brownian diffusion, E_B is given by [12, 25]

$$E_B = 1.88 Re^{-1/2} Sc^{-2/3}, \tag{5}$$

where $Sc = \nu/D_B$ is the Schmidt number, ν is the air kinetic viscosity, and D_{B} is the diffusivity for particle concentration in air obtained from Brownian motion and given by

$$D_B = C_{\mathrm{C}} k_{\mathrm{B}} T / \left(3\pi\mu d_{\mathrm{p}}\right). \tag{6}$$

Here, k_{B} is Boltzmann constant, T is absolute temperature, μ is the dynamic viscosity of air, d_p is, as before, the particle diameter and C_{C} is the Cunningham correction factor, which can be calculated by

$$C_C = 1 + \frac{\lambda}{d_{\mathrm{p}}}\left[2.514 + 0.8\exp\left(-0.55\frac{d_{\mathrm{p}}}{\lambda}\right)\right], \tag{7}$$

where λ is the mean free path of air (66 nm at a temperature of 20 °C). For UFP, the D_B is much larger than the molecular diffusion of gases in air with Schmidt number near unity.

Ground deposition is modeled by imposing a flux boundary condition based on the pipe flow analogy approach for particle deposition onto rough solid boundaries proposed by Feng [11]. The surface flux is calculated via

$$F_s = -V_{d,s}\tilde{C}_1 = -Sc^{-0.6}u_{*,\mathrm{sfc}}\tilde{C}_1, \tag{8}$$

where $\tilde{C}_1$ is the resolved particle concentration at the first vertical grid point, $V_{d,s}$ is the particle deposition velocity, and $u_{*,\mathrm{sfc}}$ is the friction velocity calculated based on the velocity at the first vertical level deep inside the canopy, and it characterizes the momentum transfer between the first level and the ground (and is thus much smaller than the friction velocity at the top of the canopy u_*). For the ground deposition, turbophoresis and impaction are neglected in this model due to the small sizes of UFP.

The assumption of massless particles leads to a set of equations (3)–(8) in which particle size appears only in the calculation of the particle diffusivity due to Brownian motion, impacting the sink term in the equation for particle transport (3) and on the deposition velocity at the ground surface given by Equation (8). In the next section, simulations are performed for a range of particle sizes all in the UFP range. In practice, this means that Equation 3 is

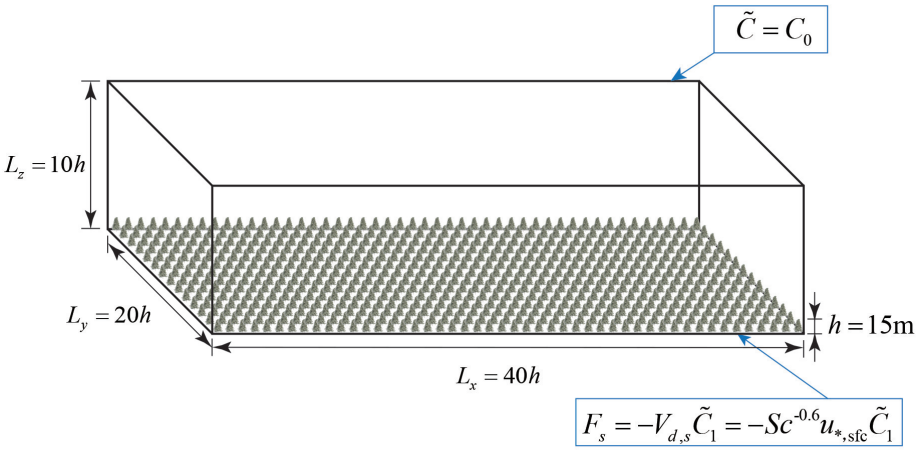

Figure 1: The computational domain with dimensions $40h \times 20h \times 10h$ used in all the LES runs. All lateral boundary conditions are periodic. Boundary conditions for particle concentration in the top and bottom surfaces are also shown in the figure.

solved separately for each particle size, and the only difference between solutions for different particle sizes is associated with the deposition processes.

The particle transport equation is discretized using a finite-volume approach with a third-order bounded scheme for the advection term [7], and the SGS particle concentration flux is closed using a flux-gradient model with a constant SGS Schmidt number equal to 0.4 [8]. The particle concentration field is initialized from a zero-concentration condition, and concentrations are driven by a constant particle concentration $\tilde{C} = C_0$ prescribed at the top of the domain (the specific choice of C_0 is not relevant, since all the concentrations and particle fluxes scale linearly with C_0) as illustrated in Figure 1. Periodic boundary conditions are used in the horizontal directions.

2.3. Simulation setup

2.3.1. Simulation of SMEAR II field experiments

To assess model skill, a simulation reproducing conditions for the field measurement campaign at SMEAR II Station for Measuring Ecosystem-Atmosphere Relations located in a Scots pine stand (*Pinus sylvestris L.*) in Southern Finland

was performed. Hereafter, this simulation is referred to as SMII. Details of the measurement site and relevant turbulence statistics based on data collected in 2005 are presented in Launiainen et al. [23] and Katul et al. [21]. Based on the SMEAR II site description, a horizontally homogeneous canopy with height $h = 15\,\mathrm{m}$ and all-sided leaf area index (LAI) 7 $\mathrm{m}^2\ \mathrm{m}^{-2}$ concentrated between 7 and 15 m above the surface [23] is assumed. The leaf area density (LAD) profile $a(z)$ used by Katul et al. [21], which includes an additional near ground peak with LAI 1.4 $\mathrm{m}^2\ \mathrm{m}^{-2}$ to model the understory layer (see Fig. 2(a)) is employed. As the effect of the understory vegetation was represented in the model by the drag force, a roughness height $z_0 = 0.001\,\mathrm{m}$, corresponding to ground roughness, is used as the bottom boundary condition.

The UFP data used here was collected between March and November 2008 at the same site as reported by Katul et al. [21]. Particle fluxes were measured using eddy covariance at two heights (subcanopy level at 2 m and above canopy level at 23.3 m above forest floor). The eddy covariance measurements were not size resolved, as particle concentrations were obtained from a condensation particle counter (TSI 3010 from TSI Inc.). However, size distribution was also measured with a differential mobility particle analyzer (DMPS), allowing for the results to be displayed as a function of the median diameter, providing pseudo size-dependent flux and deposition velocity measurements [15]. This should be kept in mind when comparing simulation of mono-dispersed particles with observations (this is particularly relevant because the deposition does not scale linearly with particle size). Field data were split into runs of 30 min and statistics were calculated for each run. Data from all runs were averaged together based on the median particle diameter and friction velocity above the canopy for each run, producing statistics as a function of friction velocity and median particle size. Only wind directions that were not contaminated upwind by the housing facility at the field site. See Katul et al. [21] for more details on data processing and selection.

The main SMII simulation was performed on a domain size of $L_x = 40h$, $L_y = 20h$ and $L_z = 10h$ with a grid spacing of $\Delta x = \Delta y = h/5$ and $\Delta z = h/15$

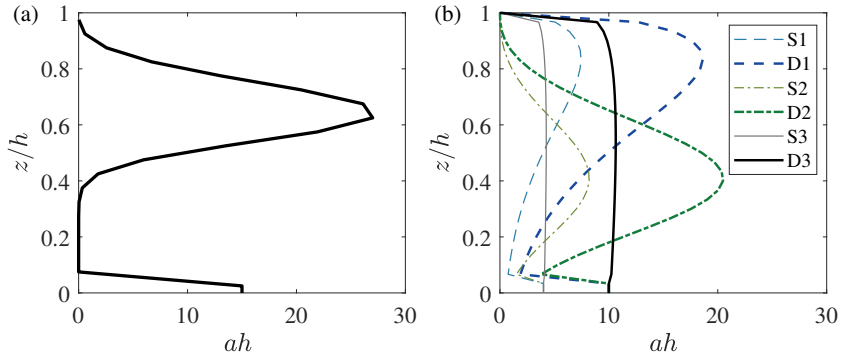

Figure 2: Leaf area density profiles for (a) the SMII simulation and (b) the 6 scenarios of idealized LAI and LAD canopies.

(see Figure 1). This domain size is typical for LES studies of canopy flows in neutral conditions, and the truncation of the atmospheric boundary layer at $L_z = 10h$ does not have significant effects on the turbulence statistics in the region $z/h \leq 2$ (e.g., see detailed studies by Bailey and Stoll [4] and Pan et al. [29]). Two additional simulations, one doubling the domain extent in all 3 directions (SMII-Large) and the other using a slightly finer grid resolution in the vertical direction (SMII-Fine with $\Delta z = h/20$) were also performed to confirm that the choice of domain size and grid resolution were appropriate.

The simulation SMII was run for a total time $T = 40L_z/u_s$ (L_z/u_s is the eddy turnover time) with the first half used to ensure the development of an approximately statistically steady-state condition for the turbulence and particle fields and the second half used for data collection. For this simulation, a $u_s = 0.52\,\mathrm{m/s}$ is used (note that this is not the actual friction velocity, defined here based on the momentum flux at the top of the canopy, but it is close in value). Because the focus is on UFP, five particle diameters equally spaced between 10 and 50 nm were used in the simulations. As mentioned before, this implies that Equation (3) is repeated five times in each simulation, one for each particle size. All particle sizes have the same initial condition and forcing at the top of the domain, and the differences in the results are a manifestation of the differences only in the particle deposition models given by Equations (4) and (8).

2.3.2. Exploration of LAI and LAD for planar homogeneous canopies

To explore the influence of LAI, LAD, and turbulence levels on the fluxes and deposition of UFP particles, ten additional simulations were performed based on combinations of two values of LAI (two-sided LAI = 4 for a sparse canopy and LAI = 10 for a dense canopy) and three LAD profiles (uniform, top-heavy, and middle-heavy, see Fig. 2(b) and Table 1). Following Katul et al. [20], the LAD profiles were generated from a Weibull distribution function with shape and scale parameters (b and c, respectively, listed in Table 1) based on data for a wide range of coniferous and deciduous tree species [40]. An understory canopy with the same LAD as in the uniform case is added to the top-heavy and bottom-heavy simulations, altering the total LAI for each simulation (see Table 1). Even though some of the LAD profiles chosen here do not have a clear separation between crown and understory, for purposes of comparing simulation results we use this region in the lowest model layer as a working definition of understory. For convenience, we label simulations as S (sparse) and D (dense) scenarios and refer to the different LAD profiles as 1 (top-heavy), 2 (middle-heavy), and 3 (uniform). The canopy height and all other physical parameters are the same as in the simulation SMII, except for a smaller pressure gradient force given by $u_s = 0.5\,\mathrm{m/s}$. Model domain and grid resolution are also kept the same as in SMII for consistency. To assess the effect of turbulence intensities in the results, additional simulations with canopies S1 and D1 were performed for weak ($u_s = 0.2\,\mathrm{m/s}$) and strong ($u_s = 0.8\,\mathrm{m/s}$) wind conditions. All LES runs are performed for neutral conditions, without buoyancy forces.

3. Results and Discussion

3.1. Simulation of SMEAR II Experiment

A comparison of profiles of turbulence statistics from SMEAR II and the results from simulation SMII is shown in Fig. 3. For comparison, all statistics from the LES were normalized using the simulated momentum flux at $z_{\mathrm{ref}} = 23.3\,\mathrm{m}$, so that for this comparison we define $u_{*,\mathrm{ref}} = (-\overline{u'w'}|_{z_{\mathrm{ref}}})^{1/2}$, as done

Scenario	LAI (m^2m^{-2})	h (m)	b	c	u_* (m/s)	L_s (m)
SMII	7.70+1.40	15	–	–	0.49	13.0
S1	4.24	15	0.4	1.4	0.19, 0.47, 0.76	5.7
S2	4.20	15	0.65	3.5	0.47	20.8
S3	4.00	15	4	1.1	0.47	6.8
D1	10.60	15	0.4	1.4	0.19, 0.47, 0.76	3.1
D2	10.50	15	0.65	3.5	0.47	15.4
D3	10.00	15	4	1.1	0.47	3.8

Table 1: The overall leaf area index (LAI) including crown and understory, canopy height (h), shape parameters (b and c), friction velocity at the canopy top (u_*), and the shear length scale (L_s) for all simulations employed here.

in the field observations (with $u_{*,\mathrm{ref}} = 0.48\,\mathrm{m/s}$ in the simulation). Data from observations correspond to the near-neutral conditions presented by Launiainen et al. [23], with errorbars showing one standard deviation around the ensemble mean value. Overall, the LES results are in agreement with measurements.

Before proceeding to analyze the results, a brief assessment of the effects of grid resolution and domain size on the results is in order. The most important components of the flow driving transport within and just above the canopy are the turbulent structures originating from the shear instability at the canopy top. These structures scale with the shear length scale $L_s = \overline{u}(h)/(\partial\overline{u}/\partial z)|_h$. In particular, these "eddies" have vertical size $\Lambda_z \approx L_s$ and horizontal size $\Lambda_x \approx 8L_s$ [36]. If these metrics are adopted to establish the minimum grid resolution requirements [37], the grid size should satisfy $\Delta z \leq L_S/4$ and $\Delta x = \Delta y \leq 2L_s$ (for a reasonable aspect ratio $\Delta_x/\Delta_z \leq 5$, the restriction on Δ_z is always more severe). For SMII, this is certainly the case as the conditions become $\Delta z \leq 3.25\,\mathrm{m}$ and $\Delta x = \Delta y \leq 26.0\,\mathrm{m}$ (note that the resolution used is $\Delta z = 1\,\mathrm{m}$ and $\Delta x = \Delta y = 3\,\mathrm{m}$). From the calculated values of L_s for the idealized canopy simulations (see Table 1), this grid resolution is sufficient in the horizontal directions for all simulations and it is sufficient in the vertical direction for all simulations except cases D1 and D3 for which it is borderline.

Thus, in principle, the resolution should be enough to provide reasonable results of UFP transport in the near canopy region. Nevertheless, comparisons between turbulence statistics from simulations SMII, SMII-fine, and SMII-large are also shown in Figure 3, confirming that there is very little sensitivity of turbulence to grid resolution and domain size.

A number of features of the comparison between SMII and observations are pointed out next. The weak secondary peak in mean velocity within the trunk space is reproduced by the LES (Fig. 3a), which also captures the fast decay in momentum flux in the upper canopy caused by the large LAD in that region (Fig. 3b). Streamwise and vertical velocity standard deviations are also well represented, with the exception of the vertical velocity standard deviation close to the ground surface. Note that only resolved portions of variances are shown, and it is possible that the SGS component of σ_w represents a significant portion of the total energy deep inside the canopy. It is also possible that the lack of representation of the vortex shedding in the wake of the trunks [6] results in under-prediction of the vertical velocity variance.

The skewness of streamwise and vertical velocity are under-predicted near the canopy top, but are reproduced in the rest of the canopy (Fig. 3e,f). The under-prediction in the upper canopy is likely associated with an under-prediction of strong sweeps and ejections, as documented in the LES of a corn-field by Pan et al. [29]. Pan et al. [29] found also that the absence of plant reconfiguration in the model was the primary reason for this under-prediction and proposed a velocity-dependent drag coefficient to improve agreement. In the present paper, the agreement between measured and simulated flow statistics are deemed acceptable for the purposes of UFP comparisons.

Next, profiles of mean particle concentration ($\overline{C}(z)$), vertical turbulent particle fluxes ($F(z) = \overline{w'C'}$), and local deposition velocities (defined as $V_d(z) = -F(z)/\overline{C}(z)$) are evaluated. Mean concentrations and turbulent fluxes are normalized by their values at the reference level above the canopy ($\overline{C}_{\rm ref}$ and $F_{\rm ref}$). This normalizing is in keeping with how the SMEAR-II data are presented in the literature. Since the simulation has a a friction velocity $u_* = 0.49\,{\rm m/s}$, only

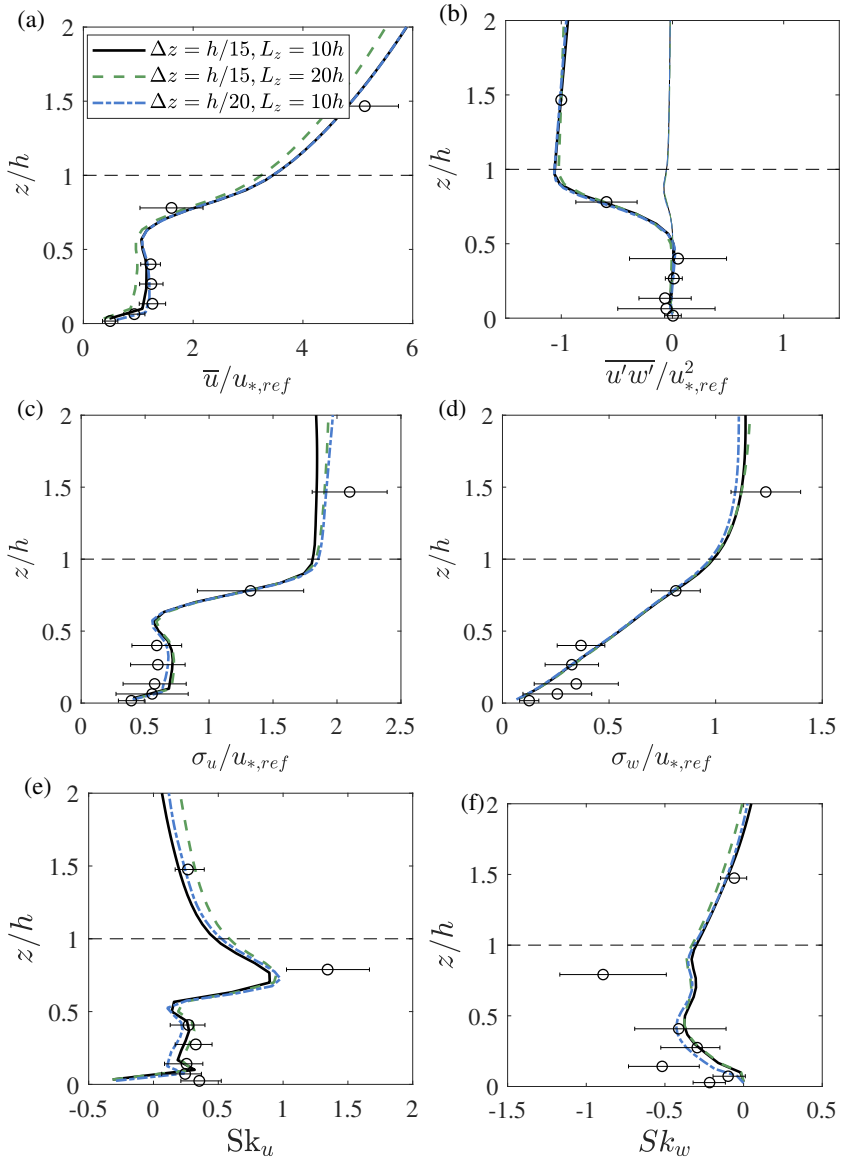

Figure 3: Comparison between LES results for simulation SMII (solid lines) and observations (open circles) of turbulence statistics for SMEAR II: (a) mean velocity, (b) momentum flux, (c) standard deviation of streamwise velocity, (d) standard deviation of vertical velocity, (e) skewness of streamwise velocity and (f) skewness of vertical velocity. The dashed line in panel (b) denotes the SGS contribution to the total momentum flux. Green dashed lines and blue dash-dotted lines indicate results from simulations SMII-large and SMII-fine, respectively.

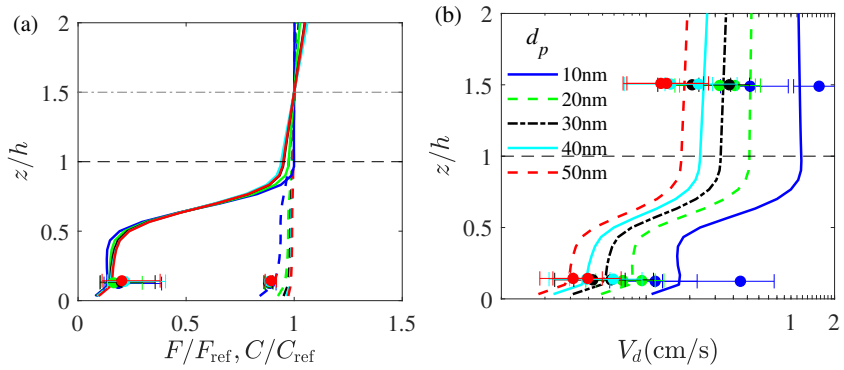

Figure 4: Comparisons between LES results (solid and dashed lines) and measurements (solid circles) for SMEAR II: (a) normalized mean particle concentration (dashed lines) and normalized mean particle flux (solid lines) and (b) deposition velocity.

field measurements obtained during periods with u_* between 0.4 and 0.7m/s were used for comparison. The observations exhibit small changes (about 10%) between the median concentrations at the reference level above the canopy and the values near the ground surface. This "well-mixed" mean concentration profile is also captured in the LES results (Fig. 4a). The large changes in particle flux with height inside the canopy, associated with the particle deposition, are also captured by the LES (Fig. 4a). The profiles of deposition velocity $V_d(z)$ highlight better the effects of particle size on deposition efficiency, showing a large reduction of deposition velocity with increasing particle diameter. The LES captured this measured trend reasonably (Fig. 4b).

The effects of particle size on UFP concentration, flux ratios, and deposition velocity are more evident in Fig. 5, where results are displayed as a function of particle size. The flux ratio, defined as the flux at the understory (or sub-canopy) level divided by the flux above the canopy displays weak dependence on the particle size. This ratio has been interpreted as the fraction of the total deposition that is contributed by the understory and ground, and the results here suggest that this fraction is not impacted by particle size in the UFP size range. As it will be clear in the next section, this effect is caused by the dense canopy crown at the SMEAR II site, which leads to small particle fluxes be-

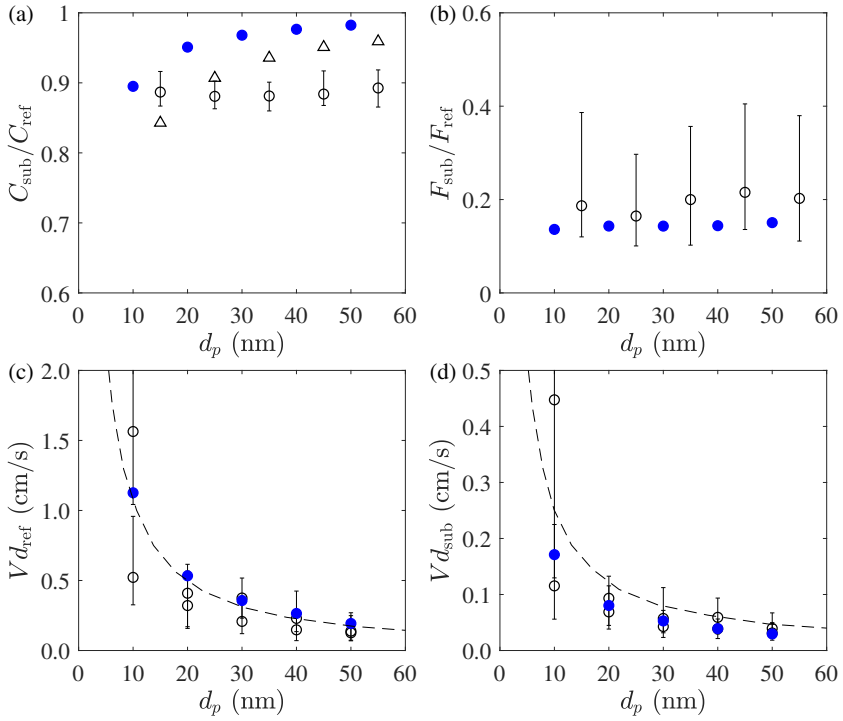

Figure 5: Comparisons between LES results (blue solid circles), 1D multilayer model from Huang et al. [17] (triangles and dashed line) and measurements (open circles) for SMEAR II: (a) deposition velocity above the canopy, (b) deposition velocity for the understory, (c) particle concentration ratio $C_{\rm sub}/C_{\rm ref}$, and (d) particle flux ratio $F_{\rm sub}/F_{\rm ref}$.

low $z/h = 0.5$ (see Fig. 4b). The SMEAR II data have significant variability, which may in part be explained by the combination of the possible variability in particle size distribution associated with any given median diameter D_p and the variability of friction velocities (both absent in the design of the numerical simulations). Finally, we note that the LES is capable of capturing the large reduction in deposition velocity between the above canopy reference height and the understory level. It also captures the reduction in deposition velocity with increasing particle size, in reasonable agreement with the SMEAR II data and with results from second-order closure modeling by Huang et al. [17].

3.2. Idealized canopy simulations

Having demonstrated the predictive skills of the LES, the effects of variable canopy LAI and LAD on UFP deposition is now explored. Fig. 6 presents the profiles of selected turbulence statistics up to third-order for the 6 idealized canopies with the purpose of characterizing the flow field and setting the stage for the discussion of UFP deposition. Hereafter, the friction velocity based on the momentum flux at the canopy top is defined as $u_* = \sqrt{-\overline{u'w'}|_{z=h}}$ and is used for velocity normalization. The complexity of the profiles displayed in Fig. 6 suggest that both LAI and LAD influence the turbulence and that no clear separation between sparse and dense canopies can be made. Some of the most relevant features of these profiles are discussed below.

Even though no clear organization between the different cases is evident, some differences become apparent when the canopy is separated into upper and lower portions at $z/h = 0.5$. In the upper canopy, the main distinction is between the bottom heavy canopies (S2 and D2) and the others (top-heavy and uniform). This is not unexpected, as in the bottom heavy canopy, the flow is not subjected to much momentum drag above $z/h \approx 0.6$. Thus, these canopies are marked by larger penetration of momentum flux (Fig. 6b), and significantly larger mean velocities (Fig. 6a) and TKE (Fig. 6c,d) in the upper canopy. In the lower canopy, the main separation is between sparse and dense canopies. This is also not unexpected, as the momentum reaching the lower canopy has already encountered a significant fraction of the total LAI, so that vertical distribution of leaf area is no longer significant.

The skewness of the streamwise velocity is used as an indication of the penetration of coherent structures [30]. Note that the profile of Sk_u has the same shape as the profile of the ratio between sweeps and ejections [e.g., see 34, 13] and the point where $Sk_u = 0$ serves as a good proxy for the maximum penetration depth of coherent structures. Similarly, the peak in Sk_u marks the region of most intense activity of coherent structures, where the ratio between momentum transported by sweeps and by ejections is maximized. This assessment is well-supported by detailed flume experiments for a rod canopy where the rod

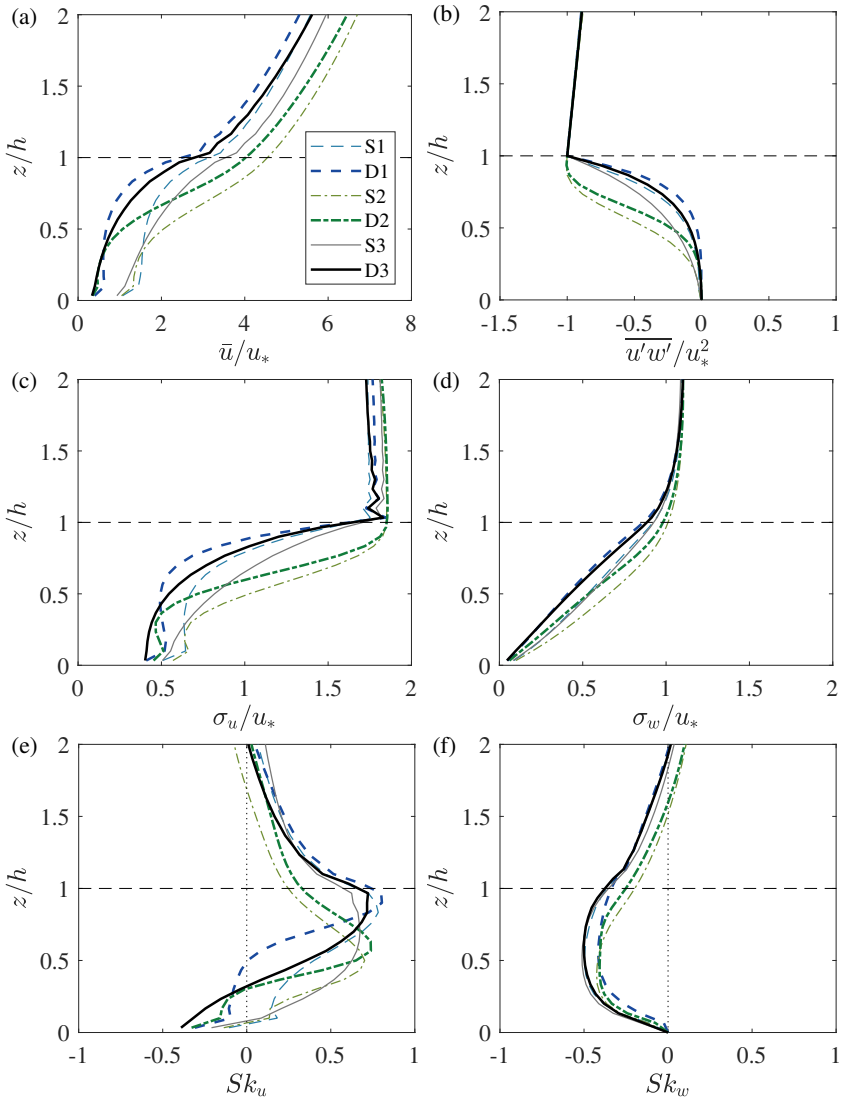

Figure 6: Turbulence statistics for idealized canopies: (a) mean velocity, (b) momentum flux, (c) standard deviation of streamwise velocity, (d) standard deviation of vertical velocity, (e) skewness of streamwise velocity and (f) skewness of vertical velocity.

density varied by more than a factor of 10 [34]. From the profiles shown in Fig. 6e, we can once again see the complex interplay between LAI and LAD, as LAD seems to be the main determinant of the position of the peak in SK_u while LAI seems to correlated better with the point where SK_u crosses zero. Based on these simulation results, the penetration depth of coherent eddies appears to be limited to the upper 40% or 50% of the canopy in the dense cases, while it extends all the way close to the ground surface in the sparse simulations. Note that for the bottom-heavy canopies, the inflection point in the mean velocity profile occurs below $z/h = 0.5$ (Fig. 6a), and an extended analysis beyond the scope of this paper would be required to establish the vertical extent of coherent eddies.

Statistics of the particle concentration field for the smallest UFP in the simulation ($Dp = 10\,\mathrm{nm}$) are displayed in Fig. 7. These results are qualitatively representative for all particle sizes simulated before. Even for neutral atmospheric conditions simulated here, the mean concentration profile for small particles can be considered to be well mixed as implied by the field experiments of Grönholm et al. [15]. The striking differences between mean velocity and concentration profiles inside the canopy are indicative of the canopy's higher efficiency in removing momentum compared to UFP removal. This is also clearly seen in the much weaker decay of particle flux with depth into the canopy when compared to the fast decay of the momentum flux. Thus, particles are more efficiently transported into the deep layers of the canopy than momentum and perhaps contribute more to the understory-forest floor deposition than their momentum counterpart.

Despite the behavior for the mean concentration profiles displaying sensitivity to LAI but not LAD shape, the profiles of particle flux and deposition velocity resemble the complexity of the turbulence statistics, and no clear organization by LAI or LAD emerges. Nevertheless, the particle deposition profiles (Fig. 7d) are sufficiently self-similar suggesting the possibility of development of reduced models for the total deposition velocity (i.e., the deposition velocity at the top of the canopy, which results from the vertically integrated deposition).

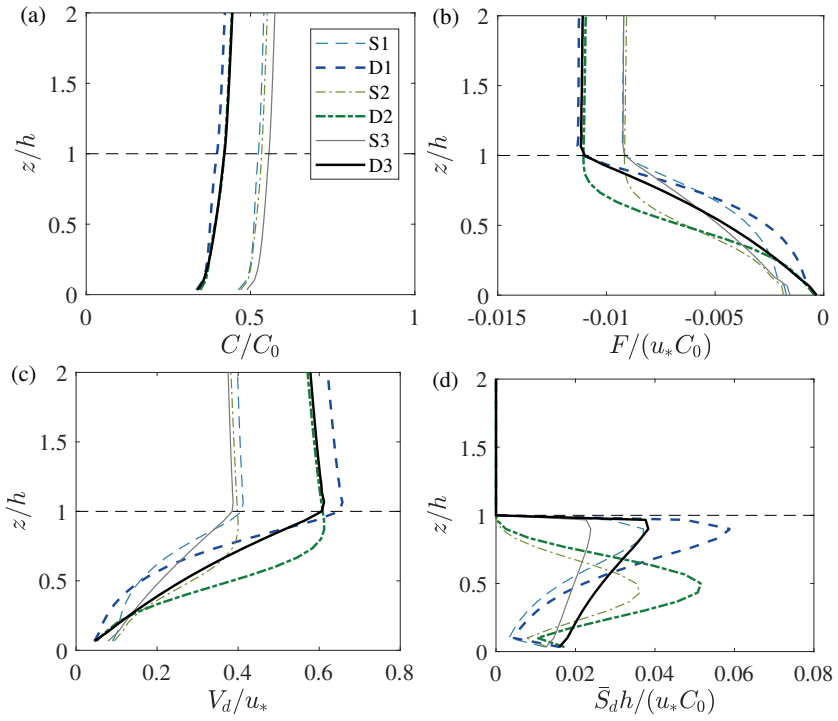

Figure 7: Particle concentration statistics for idealized canopies: (a) mean particle concentration, (b) mean particle flux, (c) deposition velocity, and (d) average canopy deposition.

Fig. 7c suggests the deposition velocity at the canopy top is almost insensitive to LAD, and it is a weak function of LAI. More specifically, a reduction of 60% in LAI (from 10 to 4) leads to a reduction of only 40% in the deposition velocity. This is a weaker effect than that found in previous studies [41, 20]. The aforementioned effect of LAI on deposition velocities is explored in more detail next.

The flux ratios are shown in Fig. 8 for all idealized canopy simulations. For the broad range of conditions tested here, the results show that: this ratio displayed a strong dependence on LAI and a mild dependence on LAD (Fig. 8a). Furthermore, for dense canopies, the ratio is approximately independent of UFP size and turbulence levels. However, for sparse canopies, both effects become important and the fraction increases with increasing UFP size and with

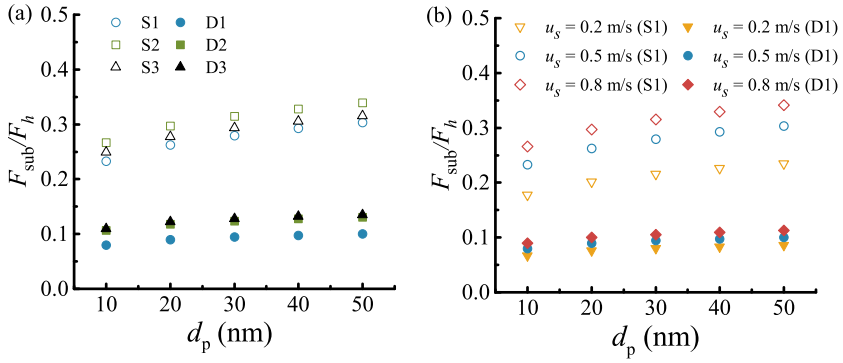

Figure 8: Ratio between particle flux at the top of subcanopy (F_{sub}) and particle flux at the top of the canopy (F_h) for (a) all canopy architecture LES using $u_s = 0.5\,\text{m/s}$ and (b) all turbulence intensity simulations for top-heavy canopies (D1 and S1).

375 increasing friction velocity.

4. A reduced model for canopy deposition

With the goal of summarizing the effects of UFP size, turbulence levels, and LAI on deposition velocity, a reduced model is now proposed. As stated in the introduction, the goal of this work is disentangling the competing effects of LAI on deposition. As noted by Slinn [39], a decrease in LAI leads to a decrease in surface area available for deposition, but also leads to an increase in the mean velocity inside the canopy, which in turn contributes to increasing deposition. The starting point is the normalized deposition velocity defined as

$$\frac{V_d}{u_*} = -\frac{F_h}{\overline{C}_h u_*}, \tag{9}$$

where $F_h = \overline{w'C'}_h$ as before. From the mean particle budget integrated over the entire canopy height,

$$F_h - F_0 = -\int_{z=0}^{h} \overline{S}_d dz, \tag{10}$$

where F_0 is the ground deposition. Adopting the same modeling approach used in the LES,

$$S_d = 1.88(d_l/\nu)^{-1/2} Sc^{-2/3} \alpha_g \tilde{C} \, |\tilde{\boldsymbol{u}}|^{1/2} \tag{11}$$

and

$$F_0 = -Sc^{-0.6} u_{*,\mathrm{sfc}} \overline{C}_0. \tag{12}$$

Because deposition velocity does not show a strong dependence on the vertical distribution of foliage (Fig. 7c), the $a(z) = LAI/h$ may be treated as a constant for this purpose and $\alpha_g = a/\pi \approx LAI/(\pi h)$. Any correlations between concentration and velocity are neglected. Hence, $\overline{\tilde{C}\,|\tilde{\boldsymbol{u}}|^{1/2}} \approx \overline{C}\overline{u}^{1/2}$ and $\overline{|\tilde{\boldsymbol{u}}|^{1/2}} \approx \overline{u}^{1/2}$. Finally, because $\overline{C}$ does not change appreciably with height inside the canopy (Fig. 7a), at least when compared to deposition velocity, it is replaced by $\overline{C}_h$. With these assumptions, the deposition velocity can be expressed as

$$\frac{V_d}{u_*} = \frac{u_{*,\mathrm{sfc}}}{u_*} Sc^{-0.6} + \frac{1.88 Re_*^{-1/2} Sc^{-2/3} LAI}{\pi h} \int_{z=0}^{h} \left(\frac{\overline{u}(z)}{u_*} \right)^{1/2} dz. \tag{13}$$

For dense forests, $(u_{*,\mathrm{sfc}}/u_*) \ll 1$ and the first term related to ground deposition can be neglected in a first-order analysis.

To make explicit the dependence of the mean velocity profile on LAI, the analytical model from Massman and Weil [27] is used assuming a constant leaf area density and is given by

$$\frac{\overline{u}}{u_*} = \frac{1}{\beta} \exp\left[-n \left(1 - \frac{z}{h} \right) \right], \tag{14}$$

where

$$n = \frac{C_d P_x LAI}{2\beta^2} \tag{15}$$

and

$$\beta = \frac{u_*}{\overline{u}_h} = a_1 - a_2 \exp(-a_3 C_d P_x LAI). \tag{16}$$

In the equation above, $a_1 = 0.32$, $a_2 = 0.264$, and $a_3 = 15.1$ are empirical constants and the values adopted here are those reported by Massman and Weil [27]. Experimental support for $a_1 \approx 0.3$ for dense canopies is discussed elsewhere [34]. Note that we add the projection term P_x in Eqns. (15) and (16) for consistency with the LES, because only this component of the LAI is providing resistance to the mean flow. If this model is used and the integral

that appears in Eqn. (13) is evaluated, then

$$\int_{z=0}^{h} \left(\frac{\overline{u}(z)}{u_*}\right)^{1/2} dz = \frac{4\beta^{3/2}h}{C_d P_x LAI}\left[1 - \exp\left(-\frac{C_d P_x LAI}{4\beta^2}\right)\right]. \tag{17}$$

The final expression for the deposition velocity follows

$$\frac{V_d}{u_*} = \left(\frac{4 \times 1.88}{\pi}\right) \frac{\beta^{3/2}}{C_d P_x Re_*^{1/2} Sc^{2/3}}\left[1 - \exp\left(-\frac{C_d P_x LAI}{4\beta^2}\right)\right]. \tag{18}$$

Note that there is a cancellation between the factor LAI/h originating from S_d (see Eqn. (13)) and its inverse originating from the integral of the mean velocity. Thus, the effect of LAI enters only through the exponential term describing the mean velocity attenuation (i.e.β). This term controls the ratio between velocity and momentum flux at the canopy top. Another interesting result embedded in Eqn. (18) is the dependence on friction velocity, given by $V_d \propto u_*^{1/2}$ instead of the linear proportionality implied by models that assume V_d/u_* to be independent of u_* (see further discussion below).

To assess the fidelity of this reduced model for deposition velocity at the canopy top, results are compared to deposition velocities directly computed from the LES in Fig. 9. Model predictions for the dense canopies are in agreement with LES results for all particle sizes (Fig. 9a). However, the model predicts deposition velocities lower than those obtained in the LES for the sparse canopies as expected. This under-prediction is associated with the ground deposition (first term on the right-hand side of Eqn. (13)). Inclusion of this term using the value of $(u_{*,\mathrm{sfc}}/u_*)$ from the LES yields predictions in good agreement with LES results for sparse canopies as well. That is, the UFP collection by the above-ground foliage remains plausible even for sparse canopies. Predictions for the canopies S1 and D1 with different levels of turbulence are also in good agreement with the LES (Fig. 9b) and model predictions for all particle sizes and all simulation conditions used here are within $\pm 20\%$ of the values obtained from the LES (Fig. 9c) despite the vertical variations in $a(z)$.

It is also of interest to evaluate the performance of the deposition model proposed by Slinn [39], given its widespread use. For UFP and adopting the reference height to be at the canopy top, Slinn's deposition model can be written

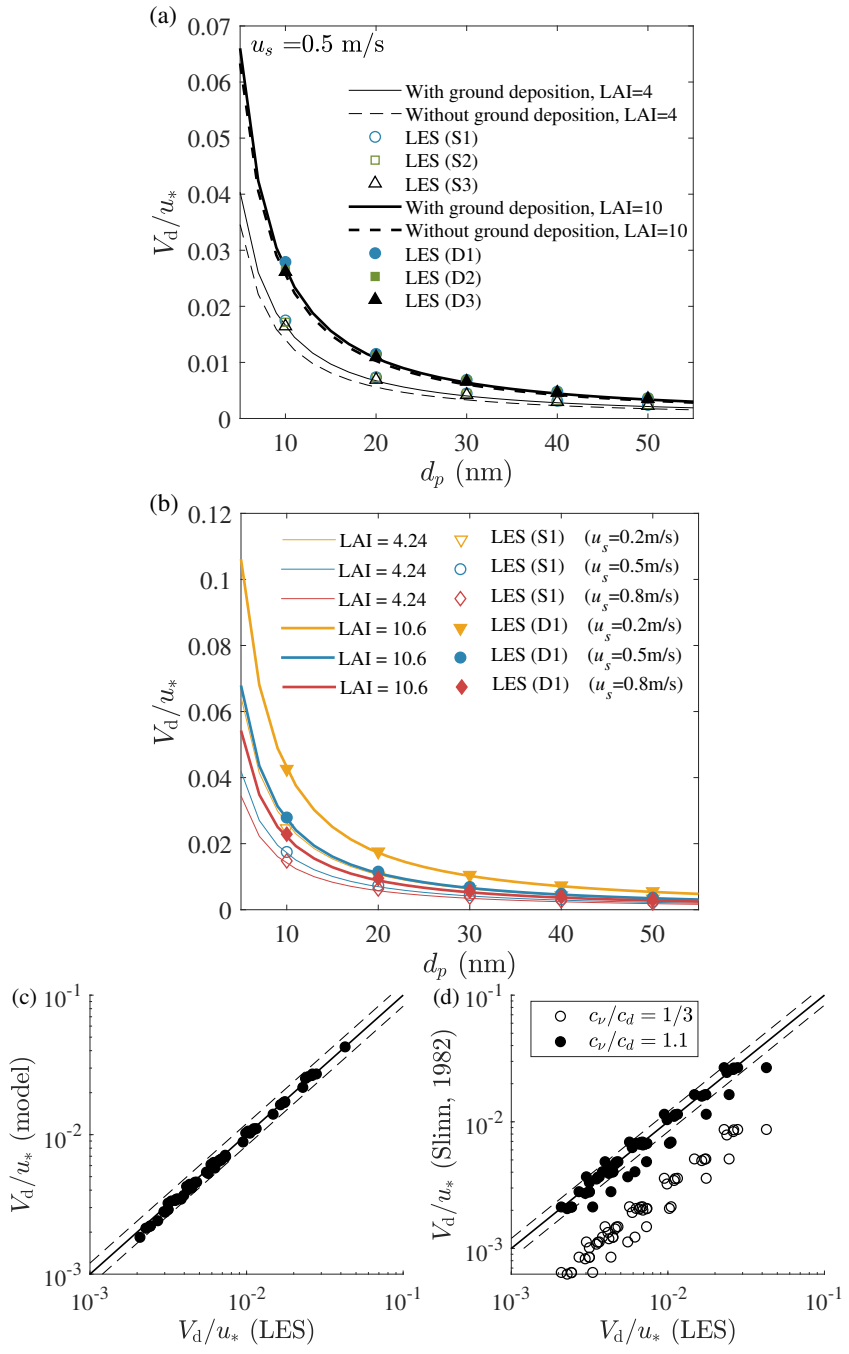

Figure 9: Comparison of deposition velocities from LES and from the proposed reduced model given by Eqn. (18) for (a) all LAI and LAD scenarios using $u_s = 0.5\,\mathrm{m/s}$, (b) all turbulence intensity simulations for top-heavy canopies (D1 and S1), and (c) all scenarios including SMII simulation. A comparison between LES results and the model proposed by Slinn [39] is also shown in panel (d). In panels (c) and (d), the solid line indicates the 1:1 line and the dashed lines indicate an error of 20%.

as

$$\frac{V_d}{u_*} = C_D \frac{\overline{u}_h}{u_*} \left[1 + \frac{1 - E_B}{E_B + E_B^{1/2} \tanh\left(\gamma E_B^{1/2}\right)} \right]^{-1}, \tag{19}$$

with $C_D = (u_*/\overline{u}_h)^2$, $E_B = (C_v/C_d)Sc^{-2/3}$, and $\gamma = [C_d a/(\kappa(h-d_0))]^{1/2}h$, with (C_v/C_d) being the ratio of viscous to total drag, κ the von Karman constant, and d_0 the displacement height. For consistency with the LES framework here, we adopt $a = P_x LAI/h$, $\overline{u}_h/u_* = 1/\beta$, and also use the model from Massman and Weil [27] to determine the displacement height. The resulting equation for V_d/u_* is independent of u_*, suggesting a linear scaling $V_d \propto u_*$. Comparison between this model and LES results is shown in Fig. 9d for $(C_v/C_d) = 1/3$ as proposed by Slinn [39] and $(C_v/C_d) = 1.1$, which fits better the LES results and is closer to the value obtained by Lin and Khlystov [26]. Nevertheless, there is significant scatter in the plot for the cases with $u_s = 0.5\,\mathrm{m/s}$. In addition, the model yields large under predictions for all particle sizes and canopy architectures (S1 and D1) under low turbulence conditions represented by $u_s = 0.2\,\mathrm{m/s}$ (these correspond to all the 10 points significantly below the $\pm 20\%$ line in the figure).

5. Conclusion and future directions

The effect of canopy morphology (foliage amounts and distribution) on UFP deposition onto vegetation elements were explored using large eddy simulations and a reduced analytical model. LES results are in agreement with published data from the SMEAR II field site in Southern Finland. The comparison is not ideal for validating the numerical implementation due to lack of truly size resolved fluxes in the observations. However, the acceptable agreement does lend confidence in the plausibility of the LES results for the turbulent flow generation and UFP deposition.

The LES results for a range of idealized canopies show that the total particle deposition and the deposition velocity at the canopy top are insensitive to the vertical distribution of leaf area but sensitive to LAI. This finding appears paradoxical given the dependence of turbulence flow statistics and in canopy

UFP fluxes on z/h_c. However, LAI does play an important role on these quantities. A number of idealized canopy simulations were undertaken that yield weaker effects of LAI on deposition velocities when compared to those inferred from other models [41, 20]. We also observed that for sparse canopies, there is non-negligible effects of turbulence intensities and particle size on the deposition velocities even in the UFP range.

A reduced analytical model is developed to explain the aforementioned observations and paradoxes for dense canopies. The analytical model describes LES deposition velocities to within 20% for all UFP sizes, turbulence conditions, and canopy architectures. The model also shows that for sparse canopies, the ground deposition is not negligible. This model may be effective in designing future LES runs or field experiments alike.

Ongoing LES development efforts will now focus on improving two aspects of the framework proposed here. On the flow generation side, accounting for waving vegetation effects on the vegetation drag coefficient is on-going to the current LES with UFP scheme used here. These revisions will presumably enhance the description of third-order flow statistics near the canopy top and expand the possibilities to explore the ejection-sweep events in momentum and UFP. The additions of thermal stratification and topographic variability is another development under consideration.

On the particle deposition side, there are a number of key features that must be added to expand the utility of the LES to address a wider set of problems. At the most basic level, the LES does not consider leaf micro-roughness and leaf shape (e.g. broad-leaves versus conifers) above and beyond smooth surfaces. Wind tunnel experiments suggest that such effects have substantial impact on UFP deposition at large LAI as discussed elsewhere [16]. Likewise, UFP charge has been entirely ignored and must be considered in future LES studies [24], perhaps using the image force method [2]. The aforementioned addition may be significant for snow-covered vegetation. Last, the imposed upper boundary condition - a constant UFP concentration and accompanying size distribution at the domain top is likely to be unrealistic during UFP growth phases. How

to include aerosol-sized particle dynamics in such high resolution canopy LES is a topic for future research.

6. Acknowledgments

This work was performed while XL was visiting UCLA with funding support from the China Scholarship Council. MC and GK were supported by the National Science Foundation (NSF-AGS-1644375 to UCLA, NSF-AGS-1644382, NSF-EAR-1344703, and NSF-DGE-1068871 to Duke University).

References

[1] Albrecht, B.A., 1989. Aerosols, cloud microphysics, and fractional cloudiness. Science 245, 1227–1230.

[2] Alonso, M., Alguacil, F., Santos, J., Jidenko, N., Borra, J., 2007. Deposition of ultrafine aerosol particles on wire screens by simultaneous diffusion and image force. Journal of Aerosol Science 38, 1230–1239.

[3] Andreae, M., Crutzen, P., 1997. Atmospheric aerosols: Biogeochemical sources and role in atmospheric chemistry. Science 276, 1052–1058.

[4] Bailey, B.N., Stoll, R., 2013. Turbulence in sparse, organized vegetative canopies: A large-eddy simulation study. Boundary-Layer Meteorology 147, 369–400. doi:10.1007/s10546-012-9796-4.

[5] Bou-Zeid, E., Meneveau, C., Parlange, M., 2005. A scale-dependent lagrangian dynamic model for large eddy simulation of complex turbulent flows. Physics of Fluids 17, 025105. doi:10.1063/1.1839152.

[6] Cava, D., Katul, G.G., 2008. Spectral short-circuiting and wake production within the canopy trunk space of an alpine hardwood forest. Boundary-layer meteorology 126, 415–431.

[7] Chamecki, M., Meneveau, C., Parlange, M.B., 2008. A hybrid spectral/finite-volume algorithm for large-eddy simulation of scalars in the atmospheric boundary layer. Boundary-layer meteorology 128, 473–484.

[8] Chamecki, M., Meneveau, C., Parlange, M.B., 2009. Large eddy simulation of pollen transport in the atmospheric boundary layer. Journal of Aerosol Science 40, 241–255. doi:10.1016/j.jaerosci.2008.11.004.

[9] Donat, J., Ruck, B., 1999. Simulated ground deposition of fine airborne particles in an array of idealized tree crowns. Boundary-Layer Meteorology 93, 469–492.

[10] Feng, J., 2008a. A size-resolved model and a four-mode parameterization of dry deposition of atmospheric aerosols. Journal of Geophysical Research: Atmospheres 113.

[11] Feng, J., 2008b. A size-resolved model and a four-mode parameterization of dry deposition of atmospheric aerosols. Journal of Geophysical Research 113. doi:10.1029/2007jd009004.

[12] Friendlander, S., 2000. Smoke, dust and haze: fundamentals of aerosol dynamics. Oxford University Press, New York, USA .

[13] Gerken, T., Chamecki, M., Fuentes, J.D., 2017. Air-parcel residence times within forest canopies. Boundary-Layer Meteorology 165, 29–54.

[14] Grönholm, T., Aalto, P.P., Hiltunen, V., llar Rannik, Rinne, J., Laakso, L., Hyvnen, S., Vesala, T., Kulmala, M., 2007. Measurements of aerosol particle dry deposition velocity using the relaxed eddy accumulation technique. Tellus B 59. doi:10.3402/tellusb.v59i3.16998.

[15] Grönholm, T., Launiainen, S., Ahlm, L., Mårtensson, E.M., Kulmala, M., Vesala, T., Nilsson, E.D., 2009. Aerosol particle dry deposition to canopy and forest floor measured by two-layer eddy covariance system. Journal of Geophysical Research 114. doi:10.1029/2008jd010663.

[16] Huang, C., Lin, M., Khlystov, A., Katul, G., 2015a. The effects of leaf size and microroughness on the branch-scale collection efficiency of ultrafine particles. Journal of Geophysical Research: Atmospheres 120, 3370–3385.

[17] Huang, C.W., Launiainen, S., Grnholm, T., Katul, G.G., 2014. Particle deposition to forests: An alternative to k-theory. Atmospheric Environment 94, 593–605. doi:10.1016/j.atmosenv.2014.05.072.

[18] Huang, C.W., Lin, M.Y., Khlystov, A., Katul, G., 2013. The effects of leaf area density variation on the particle collection efficiency in the size range of ultrafine particles (ufp). Environmental science & technology 47, 11607–11615.

[19] Huang, C.W., Lin, M.Y., Khlystov, A., Katul, G.G., 2015b. The effects of leaf size and microroughness on the branch-scale collection efficiency of ultrafine particles. Journal of Geophysical Research: Atmospheres 120, 3370–3385. doi:10.1002/2014jd022458.

[20] Katul, G., Grönholm, T., Launiainen, S., Vesala, T., 2011. The effects of the canopy medium on dry deposition velocities of aerosol particles in the canopy sub-layer above forested ecosystems. Atmospheric Environment 45, 1203–1212. doi:10.1016/j.atmosenv.2010.06.032.

[21] Katul, G.G., Grnholm, T., Launiainen, S., Vesala, T., 2010. Predicting the dry deposition of aerosol-sized particles using layer-resolved canopy and pipe flow analogy models: Role of turbophoresis. Journal of Geophysical Research 115. doi:10.1029/2009jd012853.

[22] Kulmala, M., Vehkamäki, H., Petäjä, T., Dal Maso, M., Lauri, A., Kerminen, V.M., Birmili, W., McMurry, P.H., 2004. Formation and growth rates of ultrafine atmospheric particles: a review of observations. Journal of Aerosol Science 35, 143–176.

[23] Launiainen, S., Vesala, T., Mlder, M., Mammarella, I., Smolander, S., llar Rannik, Kolari, P., Hari, P., Lindroth, A., Katul, G.G., 2007. Vertical

variability and effect of stability on turbulence characteristics down to the floor of a pine forest. Tellus B 59. doi:10.3402/tellusb.v59i5.17070.

[24] Lee, E.S., Xu, B., Zhu, Y., 2012. Measurements of ultrafine particles carrying different number of charges in on-and near-freeway environments. Atmospheric environment 60, 564–572.

[25] Lin, M., Katul, G., Khlystov, A., 2012. A branch scale analytical model for predicting the vegetation collection efficiency of ultrafine particles. Atmospheric Environment 51, 293–302. doi:10.1016/j.atmosenv.2012.01.004.

[26] Lin, M.Y., Khlystov, A., 2012. Investigation of ultrafine particle deposition to vegetation branches in a wind tunnel. Aerosol Science and Technology 46, 465–472. doi:10.1080/02786826.2011.638346.

[27] Massman, W., Weil, J., 1999. An analytical one-dimensional second-order closure model of turbulence statistics and the lagrangian time scale within and above plant canopies of arbitrary structure. Boundary-Layer Meteorology 91, 81–107.

[28] Oberdörster, G., Oberdörster, E., Oberdörster, J., 2005. Nanotoxicology: an emerging discipline evolving from studies of ultrafine particles. Environmental health perspectives 113, 823.

[29] Pan, Y., Chamecki, M., Isard, S.A., 2014. Large-eddy simulation of turbulence and particle dispersion inside the canopy roughness sublayer. Journal of Fluid Mechanics 753, 499–534. doi:10.1017/jfm.2014.379.

[30] Pan, Y., Chamecki, M., Isard, S.A., Nepf, H.M., 2015. Dispersion of particles released at the leading edge of a crop canopy. Agricultural and Forest Meteorology 211, 37–47.

[31] Pan, Y., Chamecki, M., Nepf, H.M., 2016. Estimating the instantaneous drag–wind relationship for a horizontally homogeneous canopy. Boundary-Layer Meteorology 160, 63–82.

[32] Petroff, A., Mailliat, A., Amielh, M., Anselmet, F., 2008a. Aerosol dry deposition on vegetative canopies. part i: Review of present knowledge. Atmospheric Environment 42, 3625–3653.

[33] Petroff, A., Mailliat, A., Amielh, M., Anselmet, F., 2008b. Aerosol dry deposition on vegetative canopies. part II: A new modelling approach and applications. Atmospheric Environment 42, 3654–3683. doi:10.1016/j.atmosenv.2007.12.060.

[34] Poggi, D., Porporato, A., Ridolfi, L., Albertson, J., Katul, G., 2004. The effect of vegetation density on canopy sub-layer turbulence. Boundary-Layer Meteorology 111, 565–587.

[35] Pryor, S., Gallagher, M., Sievering, H., Larsen, S.E., Barthelmie, R.J., Birsan, F., Nemitz, E., Rinne, J., Kulmala, M., Grönholm, T., et al., 2008. A review of measurement and modelling results of particle atmosphere–surface exchange. Tellus B 60, 42–75.

[36] Raupach, M., Finnigan, J., Brunet, Y., 1996. Coherent eddies and turbulence in vegetation canopies: the mixing-layer analogy, in: Boundary-Layer Meteorology 25th Anniversary Volume, 1970–1995. Springer, pp. 351–382.

[37] Ross, A.N., 2008. Large-eddy simulations of flow over forested ridges. Boundary-layer meteorology 128, 59–76.

[38] Shaw, R.H., Schumann, U., 1992. Large-eddy simulation of turbulent flow above and within a forest. Boundary-Layer Meteorology 61, 47–64.

[39] Slinn, W., 1982. Predictions for particle deposition to vegetative canopies. Atmospheric Environment (1967) 16, 1785–1794. doi:10.1016/0004-6981(82)90271-2.

[40] Teske, M.E., Thistle, H.W., 2004. A library of forest canopy structure for use in interception modeling. Forest Ecology and Management 198, 341–350. doi:10.1016/j.foreco.2004.05.031.

[41] Vesala, T., Suni, T., Rannik, Ü., Keronen, P., Markkanen, T., Sevanto, S., Grönholm, T., Smolander, S., Kulmala, M., Ilvesniemi, H., et al., 2005. Effect of thinning on surface fluxes in a boreal forest. Global Biogeochemical Cycles 19.

[42] Zhang, L., 2001. A size-segregated particle dry deposition scheme for an atmospheric aerosol module. Atmospheric Environment 35, 549–560. doi:10.1016/s1352-2310(00)00326-5.